

Received January 10, 2021, accepted January 19, 2021, date of publication January 25, 2021, date of current version February 2, 2021.

Digital Object Identifier 10.1109/ACCESS.2021.3054236

# A Novel Technique for Non-Invasive Measurement of Human Blood Component Levels From Fingertip Video Using DNN Based Models

MD. REZWANUL HAQUE, S. M. TASLIM UDDIN RAJU<sup>ID</sup>, MD. ASAF-UDDOWLA GOLAP<sup>ID</sup>,  
AND M. M. A. HASHEM

Department of Computer Science and Engineering, Khulna University of Engineering and Technology, Khulna 9203, Bangladesh

Corresponding author: S. M. Taslim Uddin Raju (taslimuddinraju7864@gmail.com)

This work was financially supported by the Khulna University of Engineering & Technology, Khulna, Bangladesh.

**ABSTRACT** Blood components such as hemoglobin, glucose, creatinine measuring are essential for monitoring one's health condition. The current blood component measurement approaches still depend on invasive techniques that are painful, and uncomfortable for the patients. To facilitate measurement at home, we proposed a novel non-invasive technique to measure blood hemoglobin, glucose, and creatinine level based on PPG signal using Deep Neural Networks (DNN). Fingertip videos from 93 subjects have been collected using a smartphone. The PPG signal is generated from each video, and 46 characteristic features are then extracted from the PPG signal, its derivatives (1<sup>st</sup> and 2<sup>nd</sup>) and from Fourier analysis. Additionally, age and gender are also included to feature because of the significant effects on hemoglobin, glucose, and creatinine. A correlation-based feature selection (CFS) using genetic algorithms (GA) has been used to select the optimal features to avoid redundancy and over-fitting. Finally, DNN based models have been developed to estimate the blood Hemoglobin (Hb), Glucose (Gl), and Creatinine (Cr) levels from the selected features. The approach provides the best-estimated accuracy of  $R^2 = 0.922$  for Hb,  $R^2 = 0.902$  for Gl, and  $R^2 = 0.969$  for Cr. Experimental aftermaths show that the proposed method is a suitable technique to be used clinically to measure human blood component levels without taking blood samples. This paper also reveals that smartphone-based PPG signal has a great potential to measure the different blood components.

**INDEX TERMS** Smartphone, non-invasive technique, hemoglobin, glucose, creatinine, NIR LED, photoplethysmogram, features extraction, features selection, deep neural networks.

## I. INTRODUCTION

Blood is the essential life-maintaining fluid that strews over the whole body and is responsible for carrying heat, hormones, antibodies, immune cells, etc. necessary for every cell. Everything related to the life cycle depends on blood directly or indirectly. As a result, the measurement and analysis of blood component levels can indicate the possibility of numerous diseases. Too much glucose level in the blood indicates the possibility of diabetes. Diabetes is the most common chronic, metabolic disorder and the leading cause of death in the worldwide [1]. Patients with long-time diabetes can be affected by several diseases like heart disease, kidneys damage, and lead to blindness [2]. Complications that occur due to diabetes can be minimized by regular monitoring of

blood glucose level. Similarly, hemoglobin is the protein molecule in red blood cells, and low hemoglobin count is the reason behind anemia [3]. So, continuous measurement of blood hemoglobin level is essential for the treatment of anemic patients [4] and premature babies [5], and dengue fever [6]. Likewise, the elevated level of creatinine intends weakened kidney [7]. So, for evaluating one's medical condition, it is imperative to measure the blood component levels regularly.

Blood component levels measurement techniques can be grouped into invasive, minimally-invasive and non-invasive [8]. Conventional measurement techniques require a blood sample of patients which is collected using finger-prick or venepuncture [9]. These methods are painful, inconvenient and costly for the patient due to frequent blood collection, and do not allow real-time monitoring [10], [11]. However, invasive techniques are more precise and reliable, but it

The associate editor coordinating the review of this manuscript and approving it for publication was Christian Pilato<sup>ID</sup>.

needs a well-resourced laboratory with trained personnel, most of whom are inaccessible in a remote area [12]. On the contrary, the non-invasive technique needs only a bio-signal (image or spectrum) to estimate the blood component levels. Non-invasive technology can overcome the above shortcomings and has become a more popular topic in smart health-care research [13]. Several techniques already exist for this purpose, but those have some limitations like portability, relatively high cost, and poor penetration of light. So, we have been motivated to develop a system that can measure the blood component levels conveniently and painlessly.

Now, near-infrared (NIR) spectroscopy and photoplethysmogram (PPG) are most widely used to measure blood component levels non-invasively [14]. PPG is an optical measurement technique that has been applied to measure the changes in blood volume in certain parts of the body [15], [16]. It reflects the movement of blood from the heart to the fingertip. The PPG system is designed with a light source, and a photodetector, where the light source illuminates the tissues region (e.g., finger) and the detector senses the reflected light. The amount of light absorbed varies periodically according to the variations of blood volume in the circulation system and can be used to acquire the PPG signal. A lot of researches have been done based on the PPG signal to monitor different physiological parameters because of its simple, low cost, and comfortable setup [17]. For example, heart rate monitoring [18], anemia detection [19], [20], heart-rate validation [21], blood pressure estimation [22] and blood glucose level [23]. Conventionally, PPG signals are acquired using optical techniques like sensor-based device, chip, or pulse oximeters [19], [21]–[24].

Recently, several smartphones which have built-in sensor systems for instantaneous measurement of heart rate, oxygen saturation based on PPG signals [25]. These non-invasive techniques are not only useful for patients those required regular health monitoring but also needed for healthcare professionals. Several studies are described briefly in the literature concerning the measurement of the different blood component levels non-invasively based on smartphones and RGB analysing. Among these, Wang *et al.* developed a smartphone-based application called HemaApp using Nexus-5p to predict the hemoglobin concentration in blood in 2016 [26]. In 2017, the same authors used Nexus-6p and updated the hardware configuration for the same purpose [3]. In 2018, Hasan *et al.* developed a smartphone application called SmartHeLP using Nexus-4p to measure the hemoglobin value [27]. In 2019, Zhang *et al.* proposed a non-invasive technique to estimate the blood glucose level based on smartphone PPG signal [28]. A few PPG signal acquisition methods have been described in the literature, but most of them used professional equipments. Therefore, we aim at using the smartphone camera and external lighting source to capture a video of the fingertip that can be used for the extraction of the PPG signal.

In this paper, a novel non-invasive technique has been proposed to estimate the blood component levels using PPG

signal characteristics features extracted from fingertip video. The finger is illuminated using near-infrared light-emitting diodes (NIR LED), and a smartphone is used to capture the fingertip video. Fingertip video is preprocessed and generated the PPG signal by applying several filtering. Analyzing the PPG signal and its derivatives signals, and using Fourier analysis on the signal, a total of 46 features are extracted. Additionally, age and gender are also included in the features set. A correlation-based feature selection (CFS) method using genetic algorithms (GA) has been used to select the appropriate features for developing DNN models. Finally, the DNN based models have been developed to estimate hemoglobin, glucose and creatinine level in blood. The major contributions of this paper are summarized as follows:

- Invoking a non-invasive system for monitoring blood glucose, hemoglobin and creatinine using smartphone which is easy to use and comfortable to patients.
- Constructing a wearable device using NIR LED for collecting fingertip video.
- Generating PPG signal from the fingertip video and extracting the PPG characteristics features from the generated PPG signal.
- Selecting appropriate features using a correlation based feature selection method to avoid redundancy in features and over-fitting problem.
- Developing DNN based models for estimating of blood component levels using both 48 features and the selected features.

The rest of this paper is organized as follows: Section II briefly described the existing works of this field. The proposed methodology, data collection, features extraction and model construction are explained in Section III. Performance analysis of our work and the comparison of results with previous works are demonstrated in Section IV. The conclusion and future direction of this paper are drawn in Section V.

## II. RELATED WORKS

The smartphone is a portable, affordable and convenient platform for developing point-of-care health tools. Non-invasive techniques are essential for patients who require to monitor blood tests regularly. In this section, we focus on the work related to measuring blood component based on PPG signals and smartphones, and summarize the representative researches as follows.

Kavsaoglu *et al.* [19] introduced a non-invasive method to predict blood Hb levels using the characteristics of the PPG signals with eight regression machine learning algorithms. Al-Baradie and Bose [29] developed a portable non-invasive Hb measurement sensor using LED for acquiring the PPG signal at the wavelength of 670 nm and 810 nm. Ramasahayam *et al.* [30] developed a system consists PPG signal acquisition module (including LEDs with wavelength of 935 nm, 950 nm, and 1070 nm and a photodetector) for the assessment of GI levels.

Wang *et al.* [26] developed a smartphone-based application as HemaApp, using the smartphone camera and multiple lighting sources, including infrared LEDs that illuminate the patient's fingertip. A smartphone Nexus-5p was used for recording a series of videos with white, 880 nm, and 970 nm LED array. They focused on three different hardware embodiments, where the first embodiments included white flash + infrared emitter, the second one consisted of incandescent lamp + white flash + infrared emitter, and the final one was made white flash + series infrared LED array. A high-band pass filter was used to calculate average intensity for each channel. Then Fast Fourier Transform (FFT) and Support Vector Machine (SVM) regression were applied for each combination of datasets. However, this is not sufficient for the people whose Hb level below 8 g/dL (heavily anemic). The limitation of HemaApp is that they collected data by using a Nexus-5 device and only one brand of the intense light bulb. Results could be varied according to the different brand devices. They achieved a correlation  $R$  result between 0.69 and 0.82, and RMSE value between 1.26 and 1.56 g/dL. Edward *et al.* [3], improved the configuration of hardware for amplifying the weaker signal of Blue and Green. They estimated the blood Hb level without using an IR LEDs. In this case, they obtained Pearson correlation of 0.62 and an RMSE of 1.27.

Anggraeni and Fatoni [31] introduced a non-invasive anemia detection system based on a digital image of palpebral conjunctiva captured by a smartphone camera. Digital image of the inferior palpebral conjunctiva was captured with an Asus Zenphone-2 Laser smartphone, ambient lighting without flash, and then color-corrected with white paper. The color intensity (R, G, B) was extracted from raw data using Colorgrab software (Loomatix), then evaluated using regression analysis. Among the three-color (R, G, B) intensity levels, red color intensity resulted in a high correlation with clinically measured Hb levels and gained  $R^2 = 0.8139$ .

Hasan *et al.* [27] developed SmartHeLP, a smartphone-based Hb level estimation technique using ANN and fingertip videos. The authors collected 10-second (300 frames) fingertip video each from 75 participants of 20-56 year of ages and the levels of Hb were from 7.6 to 13.5 gm/dL. Red, Green, and Blue pixel intensities from each frame were separated for feature extraction, and the ANN-based model was developed using these features to predict the Hb level. They observed a correlation of  $R^2$  0.93. To reduce the necessary feature space, they identified a specific Region of Interest (ROI) in the image frame.

Chowdhury *et al.* [32] proposed non-invasive GI estimation method from smartphone-based video analysis. A smartphone camera at 30 fps was used for collection the fingertip videos from 18 subjects and subsequently converted the frames of the video into PPG waveform. PPG signal was preprocessed using Gaussian filter along with Asymmetric Least Square methods and extracted features from the PPG signal. Finally, Principal Component Regression (PCR) had been applied for the prediction of GI level from the extracted

features. The proposed model could predict the glucose level with a Standard Error of Prediction (SEP) of 18.31 mg/dL.

Zhang *et al.* [28] introduced a non-invasive blood glucose estimation technique using smartphone (smartphone camera was utilized for data acquisition) PPG signals and generated an output using a machine learning algorithm (Subspace KNN classifier). A smartphone camera with a frame rate of 28 fps (sampling rate 28 Hz) was used to record a 30-40 seconds long video of the left-hand index finger. Features were extracted from a single PPG signal and its derivatives. Finally, the blood glucose level was estimated from the valid signals by applying a subspace KNN classifier. The overall accuracy was 86.2%.

Considering the existing literature, we observed that digital image or video data of eye conjunctiva and fingertip can measure different blood components such hemoglobin, glucose, and creatinine. It also shows that the PPG signal contains potential information regarding different blood components. Most of the existing techniques use specific hardware, e.g., laser light and finger chip, to acquire the PPG signal, whereas our system uses only a smartphone and an external lighting source to acquire the PPG signal. To sum up, there is up to now no non-invasive method for measuring blood component levels based on PPG signal from a fingertip video, which has the advantages of time efficiency and no calibration requirement.

### III. MATERIALS AND METHODS

In this section, the materials and methods are illustrated concisely. Collection of video data, generation of PPG signal, features extraction, features selection, and finally, model construction process have been explained briefly. The overall architecture of the system is shown in Figure 1.

#### A. EXTERNAL HARDWARE DESIGN

A wearable device has been constructed as accessories for illuminate the finger while capturing the fingertip video through smartphone. The device consists of six NIR LED with wavelength of 850 nm and, a white LED. NIR LEDs are placed in a circle with the white LED in the centre of the circle shown as Figure 2 (b). The function of the white LED is to amplify the intensity of NIR LEDs. The external surface of the device is made to black so that the reflectance factor can hardly affect the analysis. Figure 2 illustrates the prototype of the external lighting source device.

Conventionally, PPG signals are acquired using optical techniques like sensor-based device or chip. In these cases, visible or NIR LEDs are used for illuminating the finger or different parts of body tissues and a photodetector for measuring the amount of light either transmitted or reflected. Therefore, we aim to obtain PPG signals through the use of the smartphone camera to capture fingertip video and then analyzing the variation of light intensity reflected from a finger caused by the change of blood volume in systolic and diastolic cycles. Although some new smartphones are starting to be equipped with sensor or IR LEDs, the most

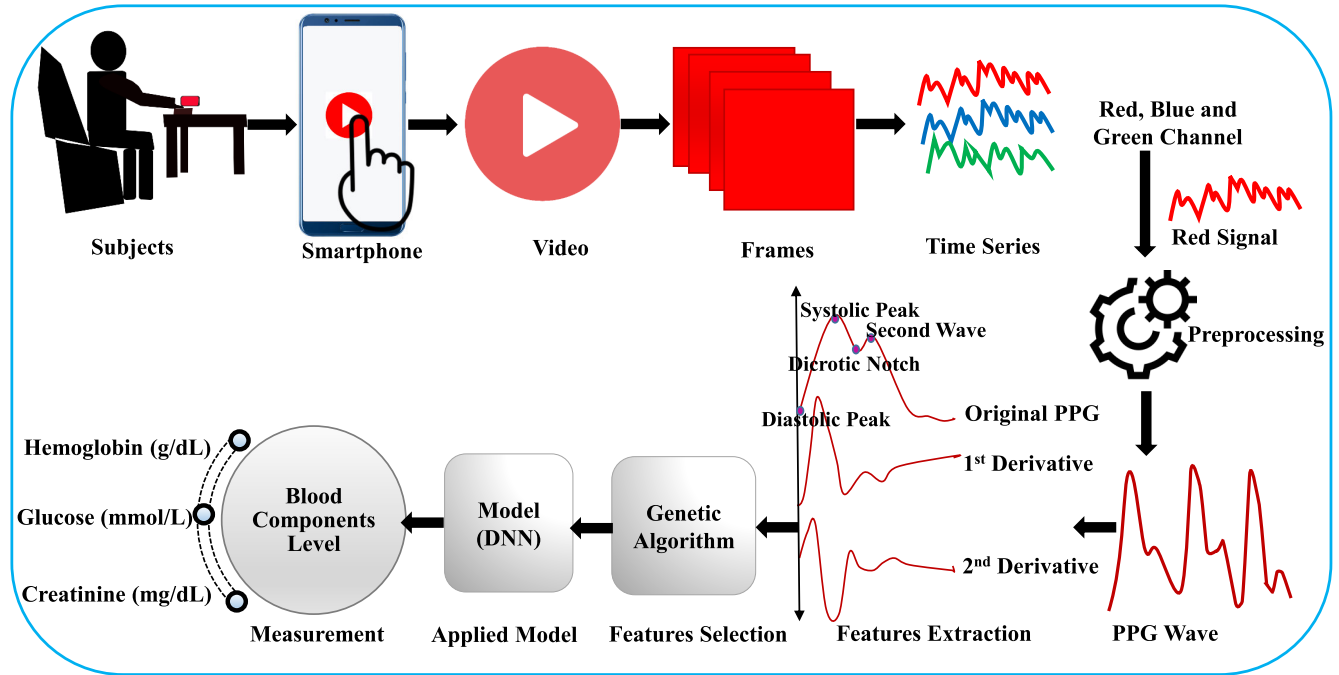


FIGURE 1. The overall system architecture of blood Hemoglobin, Glucose, and Creatinine level measurement.

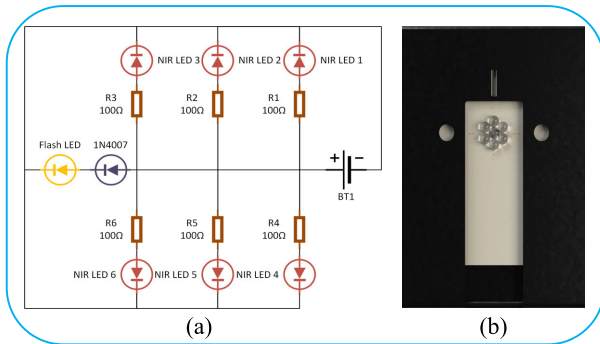


FIGURE 2. Illustration of external lighting source device: (a) Circuit diagram (b) External wearable device.

smartphone have only white LED and do not have sensors for detecting the reflected light. External lights, near-infrared lights, are required when a smartphone has no support to sense blood components non-invasively in living tissues. For fingertip-based data collection, we pointed out that a covered external NIR light source can provide the best PPG signal from a smartphone video. But the selection of near-infrared wavelength is the first step of hardware design and a critical issue to acquire the strong and clean PPG signal because we have to take wavelength as consideration for the absorption of light by blood, muscle, and skin tissues. From the study of several previously existing techniques, it is observed that most of the works used 475 – 2500 nm wavelength light for acquiring the PPG signal. For example, Ramasahayam et al. [30] were used 935 nm, 950 nm, and

TABLE 1. Patient demographics and clinical laboratory data (gold standard value/reference value).

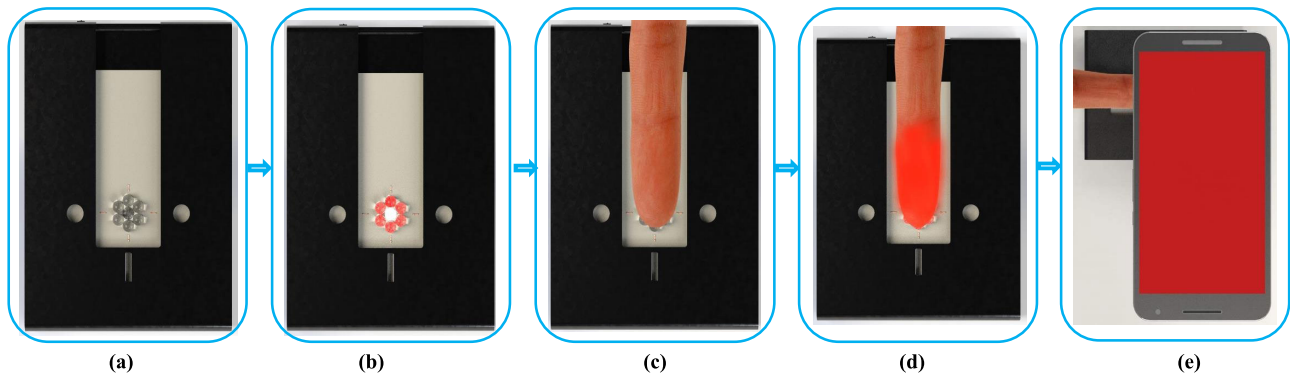
Physical Index	Statistical Data
Age (years)	33.54 ± 17.12 (0 – 79)
Gender	59 male (63.5%); 34 female (36.5%)
Hemoglobin (g/dL)	12.84 ± 2.15 (7.90 – 21.49)
Glucose (mmol/L)	6.65 ± 2.94 (3.33 – 21.11)
Creatinine (mg/dL)	1.03 ± 0.87 (0.37 – 9.02)

\* Note: Results are stated as Mean ± S.D. (range) for quantitative variables and frequency distribution (%) for categorical variables.

1070 nm NIR LED to acquire the PPG signal for estimating GI level. In HemaApp [3], 880 nm and 970 nm, as well as 500-700 nm and 1300 nm NIR LED, were used to measure the blood Hb concentration in two different studies. Al-Baradie and Bose [29] were developed a LED-based Hb sensor system for acquiring the PPG signals at the wavelengths of 670 nm and 810 nm. Light absorbed of NIR wavelength range from 700–2500 nm by tissues [17] is considerable to get the strong PPG signal as well as it can penetrate through the tissues of the finger between 1 – 2 cm effectively [33]. As it is easier to get NIR LED of 850 nm wavelength, so this LED has been used in our device.

**B. DATA COLLECTION**

A 15-second video of the right index finger was recorded using a Nexus-6p camera (30 fps), while the finger was illuminated using an external wearable device. Meanwhile,



**FIGURE 3.** Data Collection procedure: (a) External wearable device (b) Power ON of the external device (c) Index finger placed on the device when the power is OFF (d) Power ON with index finger on the device (e) Capturing 15-second video using smartphone (Nexus-6p) camera and store it in this device.

gold standard data of hemoglobin, glucose, and creatinine level of these subjects were also collected using the clinical method. These two procedures were performed consecutively but separately (with an interval of less than one minute), so that the blood component levels did not fluctuate in such a short period. The gold standard value for hemoglobin was measured with Sysmex XS-800i Haematology Analyzer, and glucose and creatinine were measured with Thermo Scientific Konelab 60i, Chemistry Analyzer respectively in the clinical laboratory. The blood sample of each subject for clinical measurement was collected just before taking the fingertip video. 93 subjects (59 males and 34 females; age:  $33.54 \pm 17.12$  years) were participated in the whole procedure. Prior to the collection of data, information regarding the work and training on how to use the wearable device and smartphone to capture fingertip video were given to the healthcare workers. Table 1 shows the statistical information of these collection.

Data collection is one of the vital stages of conducting research. Data can be corrupted within a moment for a simple mistake and affect all the next processes. The following guidelines were followed while recording the fingertip video.

- The subject's right hand and fingers were clean and dry before capturing the fingertip video.
- The index finger was preferred, but other fingers were used according to the condition of the tissue if the index finger was injured.
- The fingertip video was recorded after taking clinical blood sample.
- External wearable device was constructed in a user-friendly manner so that participants can easily place the finger on the device.
- Same conditions (room temperature and light) were maintained during the acquisition of data from any participant.
- Fingertip video was recorded using Nexus-6p smartphone camera (30 fps).

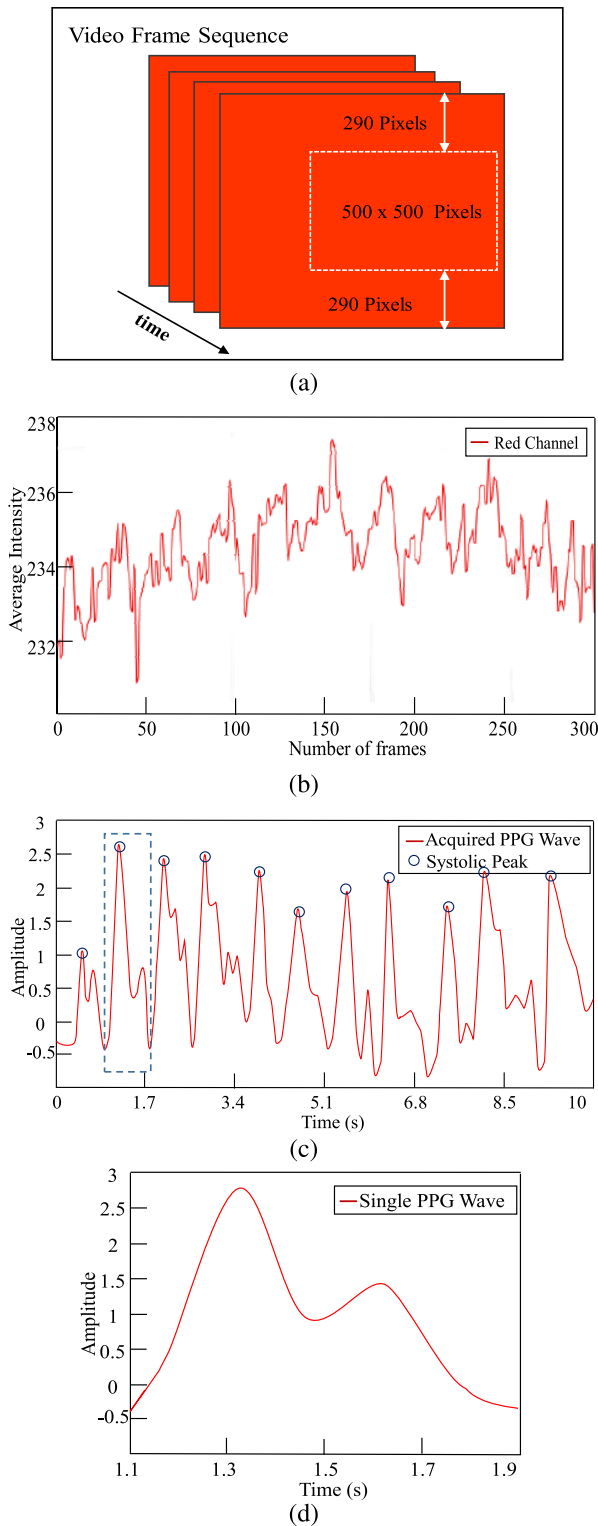
After reviewing all the facts, the right-hand index finger was placed on the wearable device and illuminating the finger with an wearable device. Finally, a 15-second video was

captured, placing a smartphone back camera on the finger, according to Figure 3. The first 3-second and the last 2-second are discarded from each fingertip video to avoid unstable frames.

### C. GENERATION OF PPG SIGNAL AND FEATURES EXTRACTION

Photoplethysmography (PPG) is a signal which is optically obtained through a plethysmograph used for detecting the volumetric variation through blood circulation [15], [16]. It reflects the movement of blood from heart to fingertip. For generating the clean and good PPG signal from the image frame, the selection of optimal Region of Interest (ROI) is indispensable [44], [45]. Another vital issue of the generation of PPG signals from the image frame is the selection of channel (Red, Green, and Blue). Because it is shown that if the range of image pixel intensity is below 200, then it is not possible to extract all characteristic features from the generated PPG signal. Among three channels, the Red channel is the highest intensity (225–245) compare to Green (0–3) and Blue (15–25). To identify the ROI, HemaApp [26] used a centre segment of the frame of an image and calculated the average intensity for each channel of the centre segment of that image, Scully *et al.* [46] picked  $50 \times 50$  array of pixels on the Green channel and Jonathan and Leahy [47] extracted  $10 \times 10$  block of the mean intensity value of the pixels from the central region. SmartHeLP [27] separated a  $10 \times 10$  pixels block from the image frame for identifying the best generated PPG signal's most adequate position. In this study, the average intensity for each channel is calculated by cropping image frame of  $500 \times 500$  pixels from right to left section of the image. This is done because the image from this section is the most consistent and stable when the video of the fingertip is captured with the smartphone.

As the PPG signal reflects the movement of blood from the heart to the fingertip, the characteristics of the PPG signal can provide information on the levels of blood constituent [19], [48]. Therefore, it is necessary to identify appropriate preprocessing and feature extraction methods to analyze the



**FIGURE 4.** Generation of PPG signal from fingertip video: (a) Crop 500 × 500 pixels from the middle of right side from each frame (b) Red channel from video’s frames (c) Continuous PPG waveform after applying Butter-worth Filter (d) One single PPG waveform with highest positive systolic peak.

PPG signal precisely [49]. A video data comprises a series of digital images called frames. 300 frames are extracted from a 10-second (30 fps) video. Then, the time series of average

**Algorithm 1** Generation of PPG Signal From Videos  
Data and Features Extraction

**Input:**  $N$ -number of videos

**Output:**  $ListFN$ -extract features for  $N$  videos

```

/* For NIR-0850 lighting condition,
capture 10sec(30fps) videos with
Nexus-6p smartphone */
/* Loop up to terminal status */
1 for  $i \leftarrow 1$  to  $N$  do
2   Extract only 300 frames for each video;
3   From right to left section of frame, measuring
   500 px as width and 500 px as height is cropped;
   /* Initialization list:  $ListH$  */
4   List of select highest intensity channel  $ListH$ ;
5   for  $j \leftarrow 1$  to 300 do
   /* Calculate  $MeanR$ ,  $MeanG$ ,
    $MeanB$  */
6   Average value of red channel  $MeanR$ ;
7   Average value of green channel  $MeanG$ ;
8   Average value of blue channel  $MeanB$ ;
9   for  $k \leftarrow 1$  to 3 do
10  if  $channel_k$  is red then
11     $MeanR \leftarrow$  average intensity for red
    channel from  $Frames_j$ ;
12  else if  $channel_k$  is green then
13     $MeanG \leftarrow$  average intensity for
    green channel from  $Frames_j$ ;
14  else
15     $MeanB \leftarrow$  average intensity for blue
    channel from  $Frames_j$ ;
   /* Calculate maximum value of
   channels */
16   $MaxvalC \leftarrow \max(MeanR, MeanG, MeanB)$ ;
   /* Append maximum value from
   three channels to list:
    $ListH$  */
17   $ListH_j \leftarrow MaxvalC$ ;
   /* Generate PPG signals:  $PPGSig_i$ 
   */
18   $PPGSig_i \leftarrow generatePPG(ListH)$ ;
   /* extract features from a
   single PPG signal and append
   features to  $ListFN$  */
19   $ListFN_i \leftarrow extractFeatures(PPGSig)$ ;
   /* Returning the extracted features
   */
20 return  $ListFN$ 

```

intensity is plotted for three channels (Red, Green, and Blue). The Red channel is the highest intensity channel. Bandpass Butterworth Filter [50] is compatible with the red channel and manages to generate a good PPG signal. So, the green and

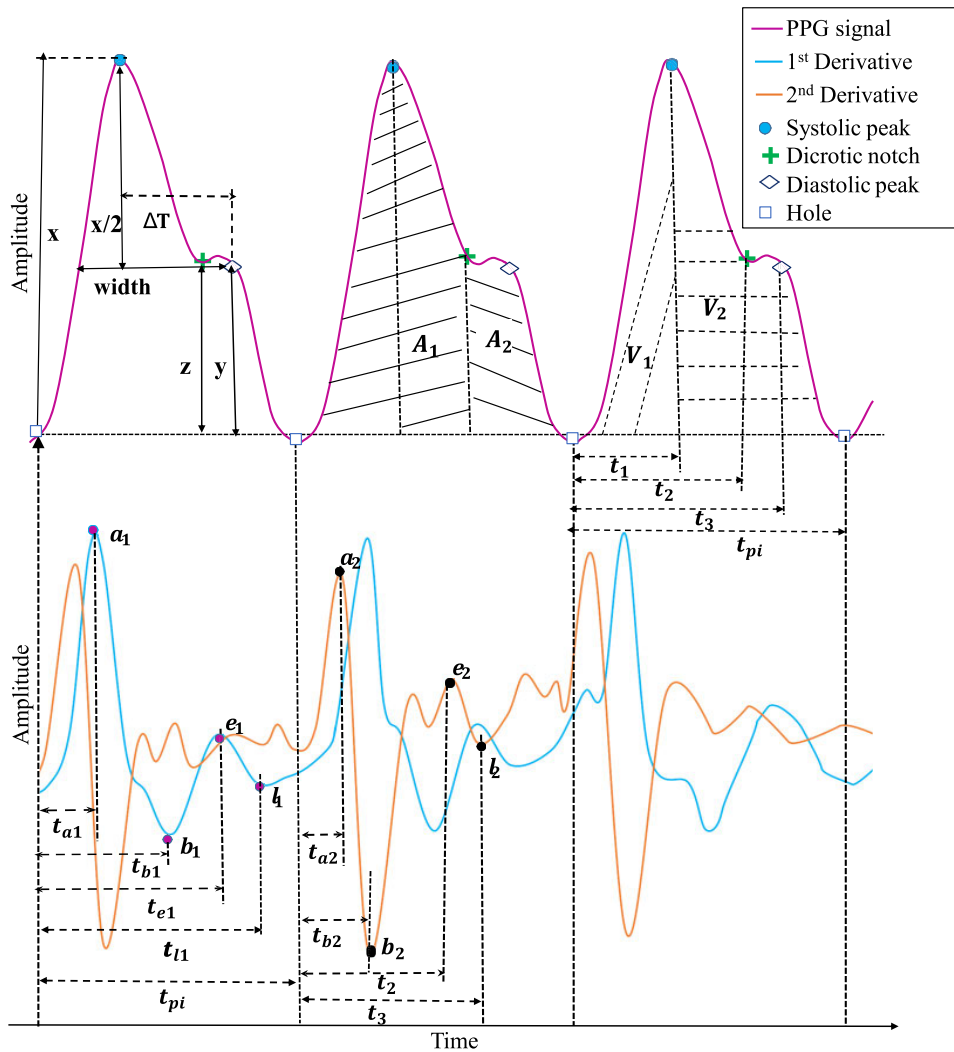


FIGURE 5. The characteristic features acquired from PPG signal and its corresponding first and second derivatives.

blue channels are discarded, and the red channel is adopted. PPG signal is continuous and repeated waveform and every individual PPG signal contains approximately same information. A peak detection algorithm is used to locate the signal peaks [51]. The signal is then divided into single periods. The waveform of single-period PPG signals might vary slightly for different people, but they are similar in terms of characteristics [28]. One single PPG signal with the highest positive systolic peak is extracted from the continuous PPG waveform because of its highest intensity changes. This single PPG signal is processed for the features extraction. The overall process of PPG signal generation from the fingertip video is demonstrated in Figure 4.

Before extraction of features, PPG signal is preprocessed to minimize noise as raw PPG signals are prone to the noise and motion artifacts. A finite impulse response (FIR) filter is applied to remove noise. Then 46 characteristics features are extracted from the PPG signal and its derivatives, shown in Figure 6. The pipeline of the PPG signal generation from

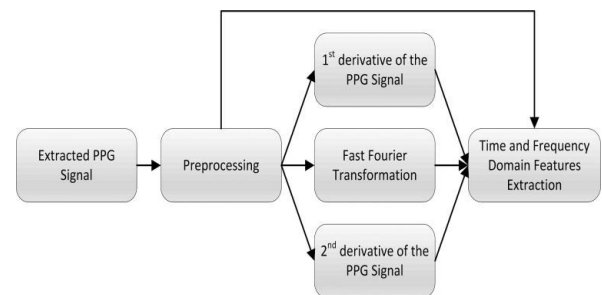


FIGURE 6. Block diagram of feature extraction.

video data and features extraction process is described algorithmically in Algorithm 1. These features have been classified as follows: 21 ( $f_3$  to  $f_{22}$  and  $f_{48}$ ) features are extracted from the PPG signal, 19 ( $f_{23}$  to  $f_{41}$ ) features extracted from 1<sup>st</sup> and 2<sup>nd</sup> derivatives [52], and 6 ( $f_{42}$  to  $f_{47}$ ) features extracted using Fourier analysis (Fast Fourier Transformation).

TABLE 2. Extracted characteristics features from PPG signal.

Features	Definition	Features	Definition
$f_3: x$	Systolic peak [34]	$f_{26}: t_{l_1}$	Interval time from point $l_1$ to next point $l_1$
$f_4: y$	Diastolic peak [34]	$f_{27}: t_{a_1}/t_{p_i}$	Ratio between time interval of $a_1$ ( $t_{a_1}$ ) and pulse interval ( $t_{p_i}$ )
$f_5: z$	Dicrotic notch	$f_{28}: t_{b_1}/t_{p_i}$	Ratio between time interval of $b_1$ ( $t_{b_1}$ ) and pulse interval ( $t_{p_i}$ )
$f_6: t_{p_i}$	Pulse interval [35]	$f_{29}: t_{e_1}/t_{p_i}$	Ratio between time interval of $e_1$ ( $t_{e_1}$ ) and pulse interval ( $t_{p_i}$ )
$f_7: y/x$	Augmentation index [36]	$f_{30}: t_{l_1}/t_{p_i}$	Ratio between time interval of $l_1$ ( $t_{l_1}$ ) and pulse interval ( $t_{p_i}$ )
$f_8: (x - y)/x$	Alternative augmentation index [37]	$f_{31}: b_2/a_2$	Ratio of $b_2$ and $a_2$ [36], [38]
$f_9: z/x$	Ratio of dicrotic notch and systolic peak [39]	$f_{32}: e_2/a_2$	Ratio of $e_2$ and $a_2$ [36], [40]
$f_{10}: (y - x)/x$	Negative relative augmentation index	$f_{33}: (b_2 + e_2)/a_2$	Ratio of $(b_2 + e_2)$ and $a_2$ [40]
$f_{11}: t_1$	Systolic peak time	$f_{34}: t_{a_2}$	Interval time from point $l_2$ to next point $a_2$ for second derivative of PPG
$f_{12}: t_2$	Dicrotic notch time	$f_{35}: t_{b_2}$	Interval time from point $l_2$ to next point $b_2$
$f_{13}: t_3$	Diastolic peak time	$f_{36}: t_{a_2}/t_{p_i}$	Ratio between time interval of $a_2$ ( $t_{a_2}$ ) and pulse interval ( $t_{p_i}$ )
$f_{14}: \Delta T = t_3 - t_1$	Time between systolic and diastolic peak [35]	$f_{37}: t_{b_2}/t_{p_i}$	Ratio between time interval of $b_2$ ( $t_{b_2}$ ) and pulse interval ( $t_{p_i}$ )
$f_{15}: t_1/2$	Time between half systolic peak points	$f_{38}: (t_{a_1} + t_{a_2})/t_{p_i}$	Ratio of $(t_{a_1} + t_{a_2})$ and pulse interval ( $t_{p_i}$ )
$f_{16}: A_2/A_1$	Inflection point area ratio [41], [42]	$f_{39}: (t_{b_1} + t_{b_2})/t_{p_i}$	Ratio of $(t_{b_1} + t_{b_2})$ and pulse interval ( $t_{p_i}$ )
$f_{17}: t_1/x$	Systolic peak rising slope	$f_{40}: (t_{e_1} + t_2)/t_{p_i}$	Ratio of $(t_{e_1} + t_2)$ and pulse interval ( $t_{p_i}$ )
$f_{18}: y/(t_{p_i} - t_3)$	Diastolic peak falling slope	$f_{41}: (t_{l_1} + t_3)/t_{p_i}$	Ratio of $(t_{l_1} + t_3)$ and pulse interval ( $t_{p_i}$ )
$f_{19}: t_1/t_{p_i}$	Ratio of systolic peak time ( $t_1$ ) and pulse interval time ( $t_{p_i}$ )	$f_{42}: f_{base}$	Fundamental component frequency obtained from Fast Fourier Transformation (FFT)
$f_{20}: t_2/t_{p_i}$	Ratio of dicrotic notch time ( $t_2$ ) and pulse interval time ( $t_{p_i}$ )	$f_{43}:  s_{base} $	Fundamental component magnitude acquired from FFT
$f_{21}: t_3/t_{p_i}$	Ratio of diastolic peak time ( $t_3$ ) and pulse interval time ( $t_{p_i}$ )	$f_{44}: f_{2nd}$	Second component frequency obtained from FFT. Such that, $f_{base} < f_{2nd}$
$f_{22}: \Delta T/t_{p_i}$	Ratio of time between systolic and diastolic peak ( $\Delta T$ ) and pulse interval time ( $t_{p_i}$ )	$f_{45}:  s_{2nd} $	Second component magnitude acquired from FFT
$f_{23}: t_{a_1}$	Interval time from point $l_1$ to point $a_1$ for 1 <sup>st</sup> derivative of PPG	$f_{46}: f_{3rd}$	Third component frequency obtained from FFT. Such that, $f_{base} < f_{2nd} < f_{3rd}$
$f_{24}: t_{b_1}$	Interval time from point $l_1$ to point $b_1$	$f_{47}:  s_{3rd} $	Third component magnitude acquired from FFT
$f_{25}: t_{e_1}$	Interval time from point $l_1$ to point $e_1$	$f_{48}: sVRI = V_2/V_1$	Stress-induced vascular response index [43]

In addition, Age ( $f_1$ ) and Gender ( $f_2$ ) of each subject are included as features. Figure 5 is shown features with characteristics point of PPG signal. The extracted features have been listed in Table 2.

D. FEATURES SELECTION

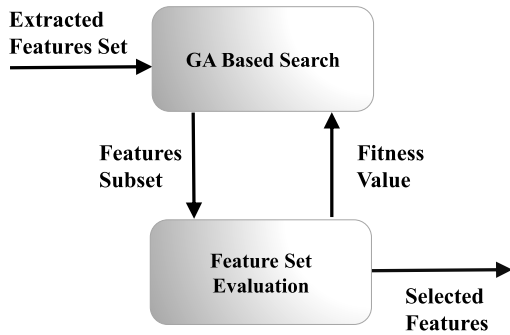
Feature selection is the most important step before model construction since the prediction power of the model depends on the features. Feature selection has lots of advantages before developing the model like it avoids the opportunities of model overfitting, improves the model accuracy by discarding the redundant features, and reduces the complexity of the algorithm and hence model trains faster. To discard redundant and irrelevant features before construction of the model and to determine the optimum subset of features, a selection process should be applied [22]. There are a number of feature

selection methods to select the optimal features set. In this work, a correlation-based feature selection (CFS) using a genetic algorithm (GA) is applied [53]. It works based on the genetic algorithm. Genetic algorithm is a search-based optimization technique derived from the biological phenomenon of natural selection [54]. It is started with a population of individuals. Every individual is capable of reaching the goal. The initial population is produced by randomly choosing of leaf nodes (variables) and functions. According to the problem, the variable and function are changed. By applying crossover and mutation techniques, the old population is replaced with a new generation. The crossover brings together two individuals into one individual. The mutation strategy switches the selected individual’s function node and generates a new individual. The features selection process has been described algorithmically in Algorithm 2. The extracted features set



**TABLE 3.** The selected features by means of CFS using genetic algorithm for different blood component levels.

Dataset	Selected Features																Count	
Hemoglobin	$f_1$	$f_2$	$f_3$	$f_4$	$f_5$	$f_6$	$f_{11}$	$f_{15}$	$f_{17}$	$f_{18}$	$f_{19}$	$f_{21}$	$f_{24}$	$f_{25}$	$f_{30}$	$f_{31}$	$f_{32}$	27
	$f_{35}$	$f_{36}$	$f_{37}$	$f_{40}$	$f_{41}$	$f_{44}$	$f_{45}$	$f_{46}$	$f_{47}$	$f_{48}$								
Glucose	$f_1$	$f_3$	$f_5$	$f_7$	$f_{11}$	$f_{12}$	$f_{14}$	$f_{15}$	$f_{16}$	$f_{17}$	$f_{18}$	$f_{20}$	$f_{22}$	$f_{23}$	$f_{28}$	$f_{32}$	$f_{34}$	25
	$f_{36}$	$f_{38}$	$f_{40}$	$f_{41}$	$f_{45}$	$f_{46}$	$f_{47}$	$f_{48}$										
Creatinine	$f_3$	$f_4$	$f_5$	$f_9$	$f_{10}$	$f_{15}$	$f_{16}$	$f_{17}$	$f_{19}$	$f_{24}$	$f_{26}$	$f_{28}$	$f_{29}$	$f_{33}$	$f_{34}$	$f_{35}$	$f_{37}$	24
	$f_{39}$	$f_{42}$	$f_{44}$	$f_{45}$	$f_{46}$	$f_{47}$	$f_{48}$											



**FIGURE 7.** Block diagram of feature selection.

randomly generate a subset of features as initial population. The fitness of each individual in the population is evaluated by an objective function (5) that qualifies how good a set of features is. The closer-fit features are selected and altered to create a new generation. Fitness of the new generation is calculated in the same way as the initial population and repeat the process. The search technique is applied to select the features (individuals) of each generation based on fitness. The individual with a higher fitness value has a better chance of being selected. The process terminates, when a maximum number of generations has been attained, or the population has reached a satisfactory fitness level. Overall feature selection process is illustrated in Figure 7. The probability of selecting  $j^{th}$  individual from the population is indicated in (1).

$$P_j = \frac{v_j}{\sum_{k=1}^M v_k}, \quad (1)$$

where,  $v_j$  is the value of fitness of an individual  $j$  in the population,  $M$  is the size of population.

Therefore, an appropriate fitness function is needed to evaluate fitness. Here, a correlation-based fitness function is used. Let,  $o_1, o_2, \dots, o_N$  be the response values and  $f_1, f_2, \dots, f_N$  be the corresponding  $n$ -dimensional feature set. The distance for each pair  $\{o_i, o_j\}$  of the response values can be calculated as follows:

$$E_o = e_{o_i, o_j} = o_i - o_j \quad (2)$$

At the same time, the distance between corresponding features sets can be referred as (3) and (4).

If  $E_o \geq 0$ ,

$$E_f = e_{f_i, f_j} = \sqrt{\frac{\sum_{k=1}^n (f_{i,k} - f_{j,k})^2}{n}} \quad (3)$$

**Algorithm 2** Genetic Algorithm for Features Selection.

**Input:** dataset  $D = \{f_i, o_i\}_{i=1}^m (f_i \in F, o_i \in O)$ ,  $\alpha$  = population size,  $\delta$  = crossover rate,  $\gamma$  = mutation rate,  $T$  = maximum iterations

**Output:** Optimal feature subset

```

/* Initialization */
1 Initialize population:  $P \leftarrow$  Generate randomly  $\alpha$ 
feasible solutions (subset of features);
/* Evaluate the fitness of each
solution,  $S$  in  $P$  */
2 Evaluate the initial population according to the
fitness function (5);
/* Initialize  $i \leftarrow 0$  */
3 while  $i \leq T$  or
[ $\text{argmax}_s \text{fitness}(S) < \text{fitness\_threshold}$ ] do
/* Selection */
4 Select two parents from the population using
roulette wheel selection ;
5 The probability to select each individual in the
population using (1) ;
/* Crossover */
6 Generate two offspring by crossover operation
between two parents ;
/* Mutation */
7 if  $\text{rand}(0.0, 1.0) \leq \gamma$  then
8 | Mutate the offspring solutions ;
9 Evaluate each offspring's according to the fitness
function (5);
/* Updating */
10 Update  $P \leftarrow P_S$  ;
/*  $P_S \leftarrow$  new offspring */
/* The best solution return */
11 return the best solution  $S_{best}$  from  $P$  that has the
highest fitness;
  
```

If  $E_o < 0$ ,

$$E_f = e_{f_i, f_j} = -\sqrt{\frac{\sum_{k=1}^n (f_{i,k} - f_{j,k})^2}{n}} \quad (4)$$

Finally, the correlation  $R_{cc}$  (as objective function) between  $E_f$  and  $E_o$  can be calculated as (5).

$$R_{cc} = \frac{S_{E_f E_o}}{\sqrt{S_{E_o} S_{E_o}}} \quad (5)$$

**TABLE 4. Control parameters and their values used in genetic algorithms for the feature selection process.**

Parameters	Value
Population Size	50
Number of Generation	50
Selection Method	Roulette-wheel
Crossover Type	Two-point
Probability of Crossover	0.1
Probability of Mutation	0.2

where,

$$S_{E_f E_o} = \frac{\sum_i (E_{f_i} - \bar{E}_f)(E_{o_i} - \bar{E}_o)}{n - 1}$$

$$S_{E_f} = \frac{\sum_i (E_{f_i} - \bar{E}_f)^2}{n - 1}, S_{E_o} = \frac{\sum_i (E_{o_i} - \bar{E}_o)^2}{n - 1} \quad (6)$$

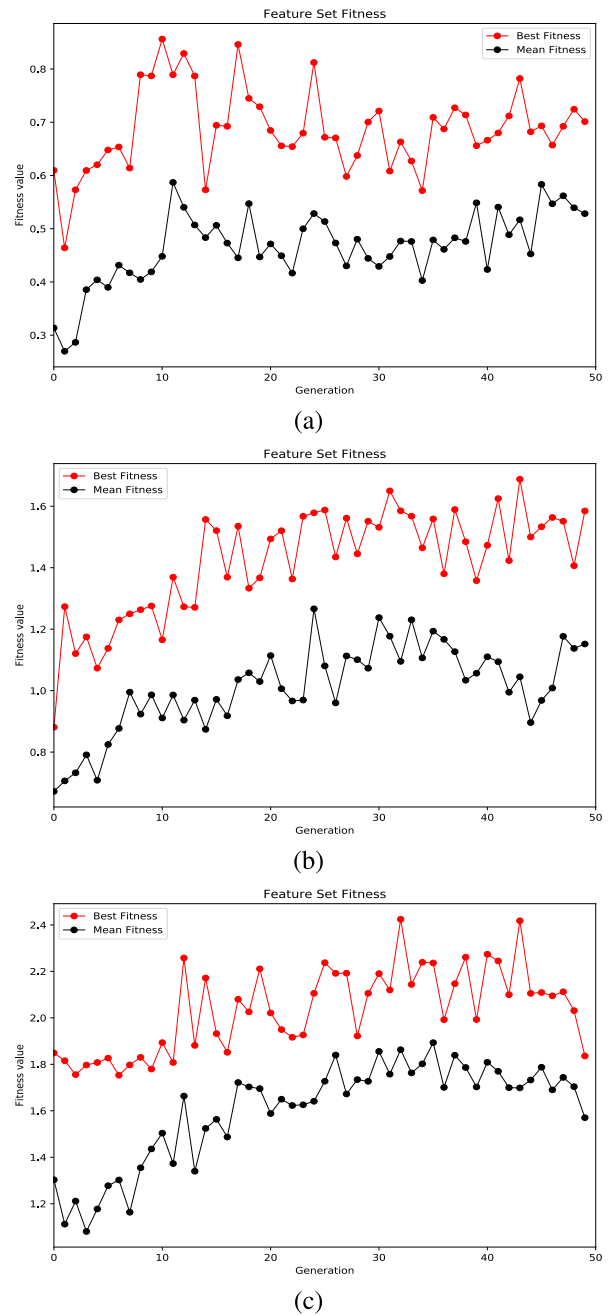
As fitness quality improves,  $R_{cc}$  becomes bigger. Hence, in this study, the optimization issue is described as maximizing the fitness function  $R_{cc}$ .

**E. FEATURES SELECTION RESULTS**

In this work, a CFS-based feature selection method has been used to discard the irrelevant and redundant features from the feature set. To select the best features subset using GA, the following control parameters are used: population size = 50, probability of crossover = 0.1, probability of mutation = 0.2, selection criteria = roulette wheel and total generation = 50 (Table 4). The improvement in features set fitness over time with the best fitness value is graphically plotted in Figure 8. The best feature subset obtained using GA for blood component levels are tabulated in Table 3. We have obtained 27 features for hemoglobin, 25 for glucose, and 24 for creatinine, and their corresponding best fitness values are 0.854, 1.642, and 2.421, respectively. From Table 3, it is shown that the hemoglobin values are varied according to age and gender. On the other hand, creatinine levels are not dependent on age and gender because abnormality of creatinine value in the blood indicates weakened kidney.

**F. MODEL CONSTRUCTION**

A Deep Neural Network is a feed-forward, artificial neural networks comprising an input layer, several hidden layers, and an output layer. It is equipped with biases, weights, and activation functions such as a rectified linear unit (ReLU) [55]. The input layer consists of neurons equal to the number of features in the dataset, and the output layer is composed of a single neuron [56]. In this work, we explored a multilayer feed-forward network, where nodes of each layer receive the inputs from the previous layer. The output of nodes in one layer will be the input of the next layer. The architecture and training procedure of DNN is illustrated in Figure 9. As shown in the figure, four hidden layers are used. There are 150 neurons in the first hidden layer and 250 neurons in the third hidden layer. There are 200 neurons with a 0.25 dropout unit in the second hidden layer and 300 neurons with a 0.50

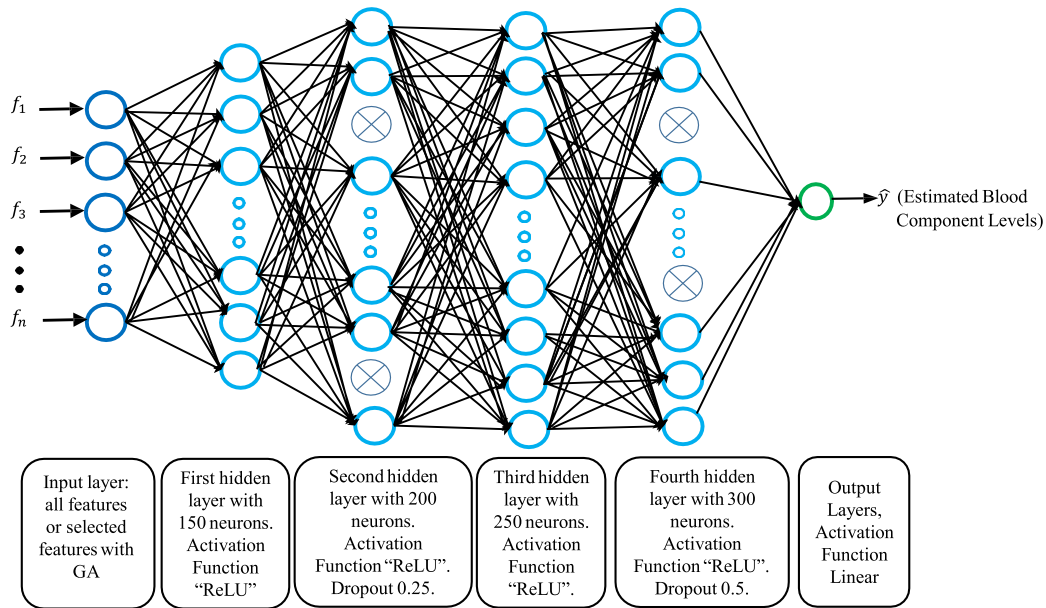


**FIGURE 8. Feature selection results: (a) Hemoglobin (Best Fitness = 0.854) (b) Glucose (Best Fitness = 1.642) (c) Creatinine (Best Fitness = 2.421).**

dropout unit in the fourth hidden layer. The dropout method is an alternative and more efficient option for addressing DNN overfitting [57]. The output of each processing unit in the hidden layer can be expressed as in .

$$q_j = \sum_j \omega_j f_j + \beta \quad (7)$$

where  $f_j$ ,  $\omega_j$  and  $\beta$  indicate input feature vector, weights and bias to the neuron respectively. The hidden layer will modify



**FIGURE 9.** The architecture of proposed Deep Neural Networks (DNN) based models for blood component levels estimation. Not all connections and units are displayed, can be marked as representative of DNN based model.

**TABLE 5.** Hyperparameters and their values used in DNN based models.

Parameters	Status
Batch size	32
Learning rate $\alpha$	0.01
The number of hidden layers	4
The number of nodes at 4 hidden layers	(150, 200, 250, 300)
Dropout at 2nd and 4th hidden layer	(0.25, 0.5)
The number of nodes at input layer	48 or selected features
The number of node at output layer	1
Activation function	ReLU, Linear
Optimizer	Adam

the input above using a nonlinear function by

$$\varphi_{re}(q) = \max(0, q) \tag{8}$$

where,  $\varphi_{re}$  is the ReLU activation function. Finally, a linear activation function is used in the output layer.

$$\varphi_{li}(q) = q' \tag{9}$$

where  $q' = (-\infty, +\infty)$

Thus, the dense layer returns the sum of the activation function. DNN model was trained on 100 epochs with respective learning rate and batch sizes as 0.01 and 32. To facilitate the training processing and update the parameter of parameters of DNN, Adam was used as optimizer function. The hyperparameters used in the proposed DNN based models are shown in Table 5. The DNN models were trained and tested with both all features and CFS-based selected features for each blood component level.

### G. TEN-FOLD CROSS-VALIDATION

In this study, a 10-fold cross-validation method was used to construct and evaluate the performances of DNN models. At first, reference Hb values and PPG characteristics features (age and gender were also included as features) of 93 subjects were divided into 10 almost equal subgroups or folds to train and test the model. In each iteration, 9 subgroups were used for training the model, and the rest one was used for testing the model. This process went on until 10 iterations were completed. After 10 times of training and testing, the reliable Hb estimation model was established. The same procedure was followed for the remaining DNN models to estimate Gl and Cr levels respectively.

## IV. EXPERIMENTAL RESULTS AND DISCUSSIONS

In this section, the experimental results and comparison of our work with previous exiting methods have been discussed briefly.

### A. PERFORMANCE EVALUATING CRITERIA

The models were implemented in Python programming language with computing environment named Spyder available in Anaconda. The experiments were carried out on a single computer (Asus X556U, Intel® Core(TM) i5 – 72000U CPU @ 2.50 GHz, 8.0 GB RAM and Nvidia GeForce 940 MX) with Windows – 10 operating system.

The performance evaluating criteria to test the performance of developed DNN based models is  $R^2$  (Coefficient of Determination),  $R$  (Pearson Correlation Coefficient), Mean Absolute Error (MAE), Mean Squared Error (MSE), Root Mean Square Error (RMSE), Mean Absolute Percentage Error (MAPE), and IA (Index of Agreement) values.

**TABLE 6.** Performance measurement of blood component levels using DNN based models with all features.

Blood Component	Algorithm	With 48 features (All features)						
		Performance measure criteria						
		$R^2$	$R$	MAE	MSE	RMSE	MAPE	AI
Hemoglobin	DNN							
	Mean	0.877	0.936	0.329	0.563	0.750	2.531	0.966
	Std. Dev.	0.031	0.018	0.045	0.140	0.059	0.319	0.013
Glucose	DNN							
	Mean	0.770	0.880	0.516	1.975	1.405	6.521	0.929
	Std. Dev.	0.042	0.032	0.083	0.486	0.113	0.986	0.020
Creatinine	DNN							
	Mean	0.865	0.993	0.072	0.100	0.316	4.834	0.975
	Std. Dev.	0.055	0.029	0.010	0.028	0.028	0.398	0.017

**TABLE 7.** Performance measurement of blood component levels using DNN based models with selected features by means of CFS-based feature selection.

Blood Component	Algorithm	With selected features via CFS ( 27 features for Hb, 25 features for Gl and 24 features for Cr)						
		Performance measure criteria						
		$R^2$	$R$	MAE	MSE	RMSE	MAPE	AI
Hemoglobin	DNN							
	Mean	0.922	0.962	0.318	0.355	0.596	2.548	0.979
	Std. Dev.	0.052	0.022	0.036	0.073	0.042	0.271	0.015
Glucose	DNN							
	Mean	0.902	0.951	0.375	0.840	0.917	5.035	0.973
	Std. Dev.	0.019	0.011	0.057	0.210	0.074	0.693	0.007
Creatinine	DNN							
	Mean	0.969	0.995	0.052	0.023	0.152	4.508	0.993
	Std. Dev.	0.037	0.026	0.005	0.005	0.012	0.298	0.020

If  $y_1, y_2, \dots, y_n$  are  $n$  reference values and  $\hat{y}_1, \hat{y}_2, \dots, \hat{y}_n$  are the corresponding estimated values, then equations for these metrics are as follows [19]:

$$R^2 = 1 - \frac{\sum_{i=1}^n (y_i - \hat{y}_i)^2}{\sum_{i=1}^n (y_i - \bar{y})^2} \tag{10}$$

$$R = \frac{\sum_{i=1}^n (f_i - \bar{f})(y_i - \bar{y})}{\sqrt{\sum_{i=1}^n (f_i - \bar{f})^2 (y_i - \bar{y})^2}} \tag{11}$$

$$MAE = \frac{1}{n} \sum_{i=1}^n |y_i - \hat{y}_i| \tag{12}$$

$$MSE = \frac{1}{n} \sum_{i=1}^n (y_i - \hat{y}_i)^2 \tag{13}$$

$$RMSE = \sqrt{\frac{1}{n} \sum_{i=1}^n (y_i - \hat{y}_i)^2} \tag{14}$$

$$MAPE = \frac{1}{n} \sum_{i=1}^n \left| \frac{y_i - \hat{y}_i}{y_i} \right| \tag{15}$$

$$IA = 1 - \frac{\sum_{i=1}^n (y_i - \hat{y}_i)^2}{\sum_{i=1}^n (|y'_i| + |\hat{y}'_i|)^2} \tag{16}$$

where,

$$y'_i = y_i - \bar{y} \text{ and } \hat{y}'_i = \hat{y}_i - \bar{y},$$

$$\bar{y} = \frac{1}{n} \sum_{i=1}^n y_i,$$

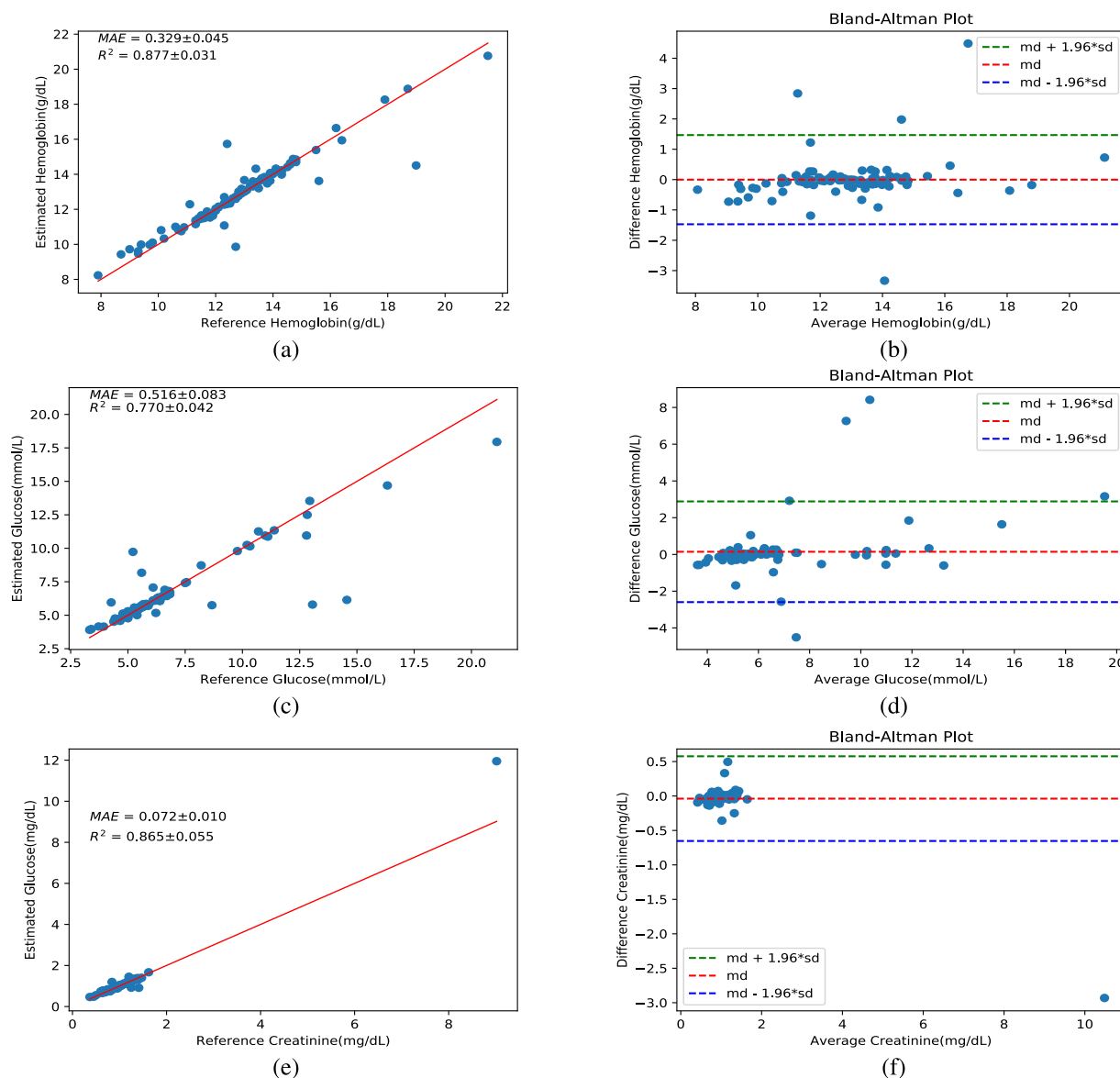
$$\bar{f} = \frac{1}{n} \sum_{i=1}^n f_i,$$

$f_i$  is the  $i^{\text{th}}$  input feature.

**B. ROBUSTNESS PERFORMANCE OF THE MODELS**

The performance of the proposed method has been evaluated with seven performance measurement indices:  $R$ ,  $R^2$ , MAE, MSE, RMSE, MAPE, and IA. It is noteworthy that the proximity of  $R^2$  to 1 indicates the strength of the relationship between model outputs and reference values. The RMSE and MSE show relative errors and MAE represent the absolute error.  $R$  and  $R^2$  for both give a correlation of blood component (Hb, Gl, and Cr) levels on datasets. The higher values of  $R^2$  indicates that the model is performed well with the input datasets.

In this study, 93 subjects were studied aged between 0 and 79 years, while 59 males and 34 females. The range of gold standard clinically measured Hb levels (Reference Hemoglobin) for this sample of individuals ranged from 7.90 g/dL to 21.49 g/dL, with Hb mean values of 12.84 g/dL and standard deviation of Hb is 2.15 g/dL. The range of clinically measured gold standard Gl levels ranged from



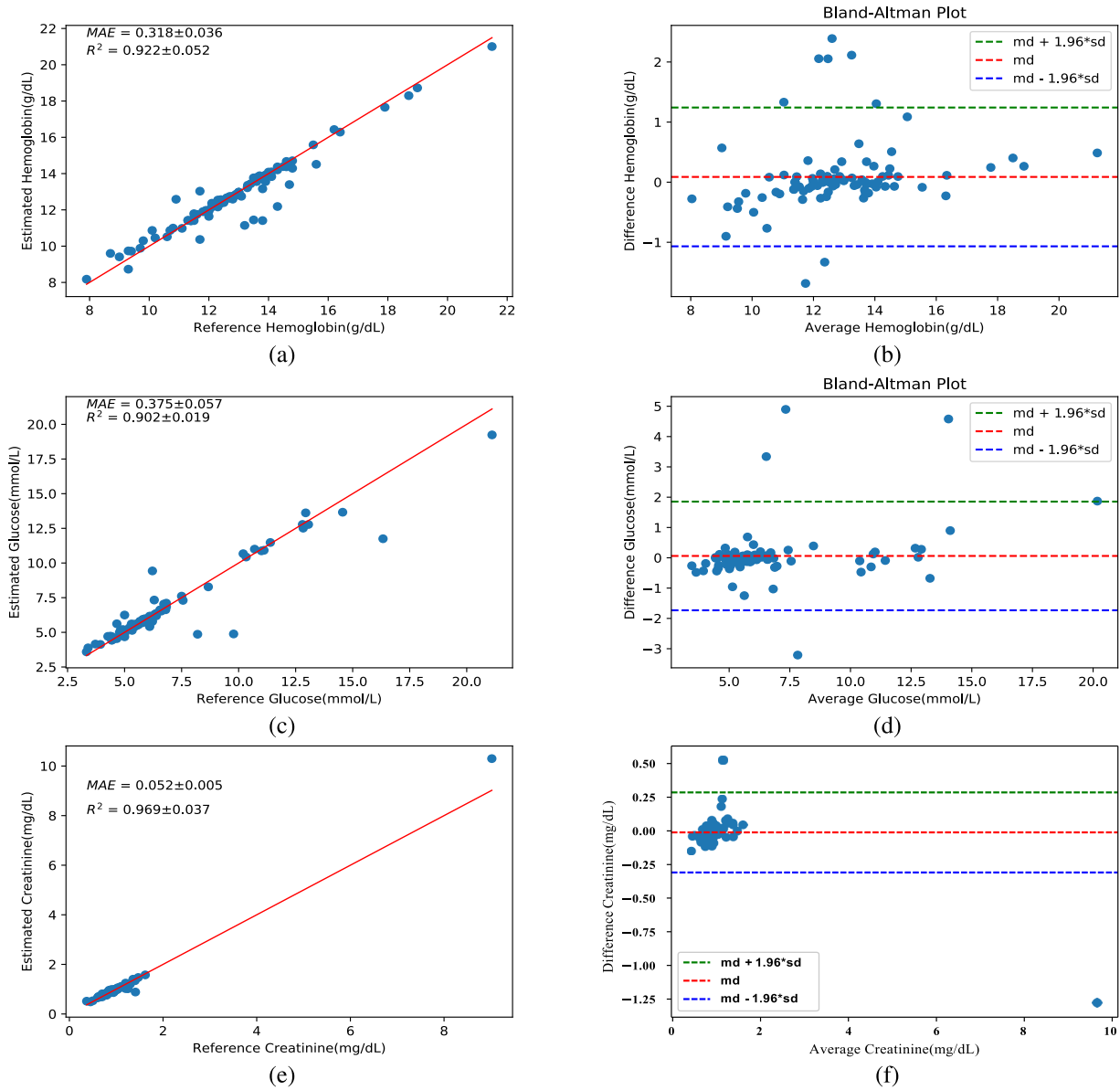
**FIGURE 10.** Relationship and agreement (Bland-Altman plot) between estimated values and reference values at testing for DNN models without feature selection.

3.33 mmol/L to 21.11 mmol/L for this individual sample, with mean GI values of 6.65 mmol/L and standard deviation of GI is 2.94 mmol/L. Similarly, for the clinically measured individual sample, the gold standard Cr levels ranged between 0.37 mg/dL and 9.02 mg/dL, with a mean of 1.03 mg/dL and standard deviation of Cr is 0.87 mg/dL.

In the first stage, the DNN based models were trained and validated with all features for each blood component level. The 10-fold cross-validation was applied to validate the DNN models. After the 10-fold cross-validation, each folds contained reference Hb values and estimated Hb values. Then the mean performances of the model were calculated. The same procedure was followed for models of estimated the GI and Cr levels. Table 6 demonstrates the results of blood component levels measurement using DNN models with all

features. The estimated accuracies of proposed DNN models are  $R^2 = 0.877$  and  $MAE = 0.329$  for Hb, 0.770 and 0.516 for GI and 0.865 and 0.072 for Cr level, respectively.

Furthermore, a correlation-based features selection (CFS) method was used to select the best optimal features. Features selection is necessary in order to reduce the probability of models over-fitting. Correlation is a measure to determine whether or not a feature is highly correlated with class label but not highly correlated with any of the other relevant features [22], [59]. After applied the CFS method to the features dataset with Hb, GI and Cr estimation levels, the number of features have been decreased from 48 to 27 for Hb level, 25 for GI level, and 24 for Cr level respectively. From Table 3, it is shown that the optimal features are varied with regard to measurement level. It is occurred due to different features are



**FIGURE 11. Relationship and agreement (Bland-Altman plot) between estimated values and reference values at testing for DNN models with CFS based feature selection.**

















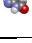

correlated to different blood component levels. In afterwards, the optimal features were applied to the DNN models to estimate the blood component levels. Models were validated using 10-fold cross-validation for each reference blood component level.


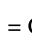


From Table 7, it can be observed that the CFS based feature selection method provided the best results when combining with DNN models for estimation of Hb, Gl, and Cr levels. According to the obtained results in Table 7, this approach provides the highest estimated accuracy of  $R^2 = 0.922$  for Hb,  $R^2 = 0.902$  for Gl, and  $R^2 = 0.969$  for Cr. From the Table 6 and Table 7, it is noticed that the accuracy ( $R^2$ ) of DNN models with CFS based selected features is increased by 5.13%, 17.14%, and 12.02% for

Hb, Gl and Cr levels comparing with DNN models with all features.

A relationship between the reference values (gold standard values) and estimated values for blood component levels has been established to understate the above results better. A correlation-based comparison between the estimated value and reference value has been shown in Figure 10 ((a), (c), and (e)) and Figure 11 ((a), (c), and (e)) for Hb, Gl, and Cr respectively. Furthermore, the Bland-Altman plot is illustrated to evaluate how much the estimated value differs from the reference value. Bland-Altman [60] plot shows the agreement between the reference value and the estimated value by constructing limits of agreement (LOA). It is found that most of the estimated values for hemoglobin, glucose,

**TABLE 8.** Comparison of our proposed DNN based models with several exiting smartphone-based non-invasive methods offered in physiological parameter monitoring processes.

Authors and Year	Purpose	Smartphone	Participants	Captured	Algorithm(s)	Performance
Dantu <i>et al.</i> (2014) [58]		HTC One X	68		–	$p - value = 0.005$
Wang <i>et al.</i> (2016) [26]		Nexus-5p	31		SVR	$R = 0.82$
Wang <i>et al.</i> (2017) [3]		Nexus-6p	32		LR	$R = 0.62$
Anggraeni and Fatoni (2017) [31]		Asus Zen-Fone 2 Laser	20		LR	$R^2 = 0.81$
Hasan <i>et al.</i> (2018) [27]		Nexus-4p	75		ANN	$R^2 = 0.93$
Zhang <i>et al.</i> (2019) [28]		iPhone 6s Plus	14		DT, BT and KNN	$Acc = 86.2\%$
Chowdhury <i>et al.</i> (2019) [32]		iPhone 7 Plus	18		PCR	$SEP = 18.31mg/dL$
<b>Proposed (In this work)</b>	<div style="display: flex; align-items: center;">    </div>	Nexus-6p	93		DNN	$\left\{ \begin{array}{l} R^2 = 0.922 \\ R^2 = 0.902 \\ R^2 = 0.969 \end{array} \right.$

\*  = Hemoglobin,  = Glucose,  = Creatinine,  = Video,  = Image,  $Acc$  = Accuracy, SVR = Support Vector Regression, LR = Linear Regression, ANN = Artificial Neural Network, DT = Decision Tree, BT = Bagged Trees, KNN = K-nearest neighbor, PCR = Principal Component Regression, SEP = Standard Error of Prediction, DNN = Deep Neural Network.

and creatinine are within the LOA (bias  $\pm 1.96 \times SD$ ) in Figure 10 ((b), (d), and (f)) and Figure 11 ((b), (d), and (f))

**C. COMPARISON OF RESULTS**

Compassion of our work is shown in Table 8 for estimating the blood component levels to validate our contribution with previous existing smartphone-based non-invasive techniques.

Looking at individual related works in Table 8, Dantu *et al.* [58] introduced a method for measuring Gl level via smartphone camera by capturing the transmitted laser light through a fingertip. The blue and green intensities of modified Beer-Lambert law was used to determine the GL level and gained a ( $p - value$ ) = 0.005. Wang *et al.* [26] developed a smartphone-based application named as HemaApp (FDA-approved device) to measure Hb level non-invasively. The authors captured fingertip video data from 31 subjects using Nexus-5p, used the SVR model, and achieved highest relationship with correlation coefficient ( $R$ ) of 0.82. In [3], the same authors improved the configuration of hardware and used the LR model, and achieved a Pearson correlation of 0.62. Anggraeni and Fatoni [31] developed LR model using conjunctiva image of 20 participants captured by Asus ZenFone 2 and estimated the Hb level that highly correlated with clinical Hb value and gained a relationship with  $R^2$  of 0.81. In [27], the authors developed a smartphone-based application named as SmartHeLP to measure the Hb concentration in blood. In this case, they collected 75 fingertip video data via Nexus-4p smartphone and applied in the ANN model, and achieved relationship with  $R^2$  of 0.93. Zhang *et al.* [28] developed a system for the

estimation of blood Gl level based on smartphone fingertip video. The authors acquired the PPG signal from video, used subspace KNN classifier and obtained the accuracy  $Acc = 86.2\%$ . Chowdhury *et al.* [32] proposed a smartphone-based approach to estimate the blood Gl level in a non-invasive. The authors recorded the fingertip video, converted the frames into PPG signal, applied PCR algorithm on the extracted features, and achieved a SEP as low as 18.31 mg/dL. However, it is difficult to compare existing works related to this filed due to different datasets, devices, and sensors to collect the data from various parts of the subject’s body and different evaluation criteria. In our proposed method, we have used a smartphone device (Nexus-6p) to capture the fingertip video data, generated PPG signal from fingertip videos, and developed DNN based models to estimate the hemoglobin, glucose, and creatinine levels and achieved a good performance.

**V. CONCLUSION**

This paper introduced a non-invasive hemoglobin, glucose, and creatinine measurement system based on PPG signal obtained from fingertip video using the DNN model. It provides a good basis for observing hemoglobin, glucose, and creatinine in real-time from home. Firstly, fingertip video is recorded using a smartphone, illuminating the finger with 850 nm NIR LED. Then, PPG signals are generated from the video. From the PPG signal, its derivatives (1<sup>st</sup> and 2<sup>nd</sup>) and Fourier analysis, 46 characteristic features are extracted. A correlation-based features selection method using a genetic algorithm is used to select appropriate features. Finally, DNN

based models are developed, and 10-fold cross-validation method is applied to validated the models. The obtained results show that the combination of CFS and DNN models are very effective for estimating blood component levels. The performance of our proposed technique has also been compared against existing methods, which indicates the applicability of our proposed method.

In the future, we would like to prefer the following approaches for further enhancement of our work: (1) the dataset will be increased from a heterogeneous people to make the dataset more balanced, (2) the video will be recorded using different smartphone to increase the reliability of the proposed technique, (3) the fingertip video collection process will be handled automatically, (4) the whole estimation process will be cloud-based, (5) the data will be captured from an end-user and sent the data to a cloud-server using a smartphone-based application as well as the result of captured data will be displayed to the end-user by analyzing the data with the models.

#### ACKNOWLEDGMENT

The authors would like to thanks all the voluntary participants of this study and Dr. Moniruzzaman, Managing Director, physicians, nurses, and supporting members from Medical Centre Hospital, Chittagong, Bangladesh, for their constant support during the study. The authors also thank anonymous reviewers for suggestions on improving this manuscript.

#### CONFLICTS OF INTEREST

The authors declare that there are no conflicts of interest regarding the publication.

#### REFERENCES

- [1] J. Li and C. Fernando, "Smartphone-based personalized blood glucose prediction," *ICT Exp.*, vol. 2, no. 4, pp. 150–154, Dec. 2016.
- [2] Z. Li, G. Li, W.-J. Yan, and L. Lin, "Classification of diabetes and measurement of blood glucose concentration noninvasively using near infrared spectroscopy," *Infr. Phys. Technol.*, vol. 67, pp. 574–582, Nov. 2014.
- [3] E. J. Wang, W. Li, J. Zhu, R. Rana, and S. N. Patel, "Noninvasive hemoglobin measurement using unmodified smartphone camera and white flash," in *Proc. 39th Annu. Int. Conf. IEEE Eng. Med. Biol. Soc. (EMBC)*, Jul. 2017, pp. 2333–2336.
- [4] S. S. Morris, M. T. Ruel, R. J. Cohen, K. G. Dewey, B. de la Brière, and M. N. Hassan, "Precision, accuracy, and reliability of hemoglobin assessment with use of capillary blood," *Amer. J. Clin. Nutrition*, vol. 69, no. 6, pp. 1243–1248, Jun. 1999.
- [5] M. K. Hasan, N. Sakib, R. R. Love, and S. I. Ahamed, "Analyzing the existing noninvasive hemoglobin measurement techniques," in *Proc. IEEE 8th Annu. Ubiquitous Comput., Electron. Mobile Commun. Conf. (UEMCON)*, Oct. 2017, pp. 442–448.
- [6] J. L. A. Nirupa and V. J. Kumar, "Non-invasive measurement of hemoglobin content in blood," in *Proc. IEEE Int. Symp. Med. Meas. Appl. (MeMeA)*, Jun. 2014, pp. 1–5.
- [7] L. Scarfe, A. Rak-Raszewska, S. Geraci, D. Darssan, J. Sharkey, J. Huang, N. C. Burton, D. Mason, P. Ranjzad, S. Kenny, N. Gretz, R. Lévy, B. Kevin Park, M. García-Fiñana, A. S. Woolf, P. Murray, and B. Wilm, "Measures of kidney function by minimally invasive techniques correlate with histological glomerular damage in SCID mice with adriamycin-induced nephropathy," *Sci. Rep.*, vol. 5, no. 1, Oct. 2015, Art. no. 13601.
- [8] S. A. Siddiqui, Y. Zhang, J. Lloret, H. Song, and Z. Obradovic, "Pain-free blood glucose monitoring using wearable sensors: Recent advancements and future prospects," *IEEE Rev. Biomed. Eng.*, vol. 11, pp. 21–35, 2018.
- [9] H. Von Schenck, M. Falkensson, and B. Lundberg, "Evaluation of 'hemocue' a new device for determining hemoglobin," *Clin. Chem.*, vol. 32, no. 3, pp. 526–529, 1986.
- [10] P. P. Pai, P. K. Sanki, S. K. Sahoo, A. De, S. Bhattacharya, and S. Banerjee, "Cloud computing-based non-invasive glucose monitoring for diabetic care," *IEEE Trans. Circuits Syst. I, Reg. Papers*, vol. 65, no. 2, pp. 663–676, Feb. 2018.
- [11] S. Lekha and S. M., "Real-time non-invasive detection and classification of diabetes using modified convolution neural network," *IEEE J. Biomed. Health Informat.*, vol. 22, no. 5, pp. 1630–1636, Sep. 2018.
- [12] M. Parker, Z. Han, E. Abu-Haydar, E. Matsiko, D. Iyakaremye, L. Tuyisenge, A. Magaret, and A. Lyambabaje, "An evaluation of hemoglobin measurement tools and their accuracy and reliability when screening for child anemia in rwanda: A randomized study," *PLoS ONE*, vol. 13, no. 1, Jan. 2018, Art. no. e0187663.
- [13] J. Harvey, S. M. A. Salehizadeh, Y. Mendelson, and K. H. Chon, "OxiMA: A frequency-domain approach to address motion artifacts in photoplethysmograms for improved estimation of arterial oxygen saturation and pulse rate," *IEEE Trans. Biomed. Eng.*, vol. 66, no. 2, pp. 311–318, Feb. 2019.
- [14] J. Kraitl, D. Klinger, D. Fricke, U. Timm, and H. Ewald, "Non-invasive measurement of blood components," in *Advancement in Sensing Technology*. Berlin, Germany: Springer, 2013, pp. 237–262.
- [15] F. Rundo, S. Conoci, A. Ortis, and S. Battiato, "An advanced bio-inspired PhotoPlethysmoGraphy (PPG) and ECG pattern recognition system for medical assessment," *Sensors*, vol. 18, no. 2, p. 405, Jan. 2018.
- [16] J. Allen, "Photoplethysmography and its application in clinical physiological measurement," *Physiol. Meas.*, vol. 28, no. 3, pp. R1–R39, Mar. 2007.
- [17] J. Yadav, A. Rani, V. Singh, and B. M. Murari, "Prospects and limitations of non-invasive blood glucose monitoring using near-infrared spectroscopy," *Biomed. Signal Process. Control*, vol. 18, pp. 214–227, Apr. 2015.
- [18] S. Kwon, H. Kim, and K. Suk Park, "Validation of heart rate extraction using video imaging on a built-in camera system of a smartphone," in *Proc. Annu. Int. Conf. IEEE Eng. Med. Biol. Soc.*, Aug. 2012, pp. 2174–2177.
- [19] A. R. Kavsaoğlu, K. Polat, and M. Hariharan, "Non-invasive prediction of hemoglobin level using machine learning techniques with the PPG signal's characteristics features," *Appl. Soft Comput.*, vol. 37, pp. 983–991, Dec. 2015.
- [20] M. A.-U. Golap and M. M. A. Hashem, "Non-invasive hemoglobin concentration measurement using MGGP-based model," in *Proc. 5th Int. Conf. Adv. Electr. Eng. (ICAEE)*, Sep. 2019, pp. 1–6.
- [21] J. Moraes, M. Rocha, G. Vasconcelos, J. V. Filho, V. de Albuquerque, and A. Alexandria, "Advances in photoplethysmography signal analysis for biomedical applications," *Sensors*, vol. 18, no. 6, p. 1894, Jun. 2018.
- [22] F. Miao, N. Fu, Y.-T. Zhang, X.-R. Ding, X. Hong, Q. He, and Y. Li, "A novel continuous blood pressure estimation approach based on data mining techniques," *IEEE J. Biomed. Health Informat.*, vol. 21, no. 6, pp. 1730–1740, Nov. 2017.
- [23] N. Nirala, R. Periyasamy, B. K. Singh, and A. Kumar, "Detection of type-2 diabetes using characteristics of toe photoplethysmogram by applying support vector machine," *Biocybern. Biomed. Eng.*, vol. 39, no. 1, pp. 38–51, Jan. 2019.
- [24] C. Choi, B.-H. Ko, J. Lee, S. K. Yoon, U. Kwon, S. J. Kim, and Y. Kim, "PPG pulse direction determination algorithm for PPG waveform inversion by wrist rotation," in *Proc. 39th Annu. Int. Conf. IEEE Eng. Med. Biol. Soc. (EMBC)*, Jul. 2017, pp. 4090–4093.
- [25] P. Schoettker, J. Degott, G. Hofmann, M. Proença, G. Bonnier, A. Lemkaddem, M. Lemay, R. Schorer, U. Christen, J.-F. Knebel, A. Wuerzner, M. Burnier, and G. Wuerzner, "Blood pressure measurements with the OptiBP smartphone app validated against reference auscultatory measurements," *Sci. Rep.*, vol. 10, no. 1, pp. 1–12, Dec. 2020.
- [26] E. J. Wang, W. Li, D. Hawkins, T. Gernsheimer, C. Norby-Slycord, and S. N. Patel, "HemaApp: Noninvasive blood screening of hemoglobin using smartphone cameras," in *Proc. ACM Int. Joint Conf. Pervas. Ubiquitous Comput.*, Sep. 2016, pp. 593–604.



- [27] M. K. Hasan, M. M. Haque, R. Adib, J. F. Tumpa, A. Begum, R. R. Love, Y. L. Kim, and I. A. Sheikh, "Smarthelp: Smartphone-based hemoglobin level prediction using an artificial neural network," in *Proc. AMIA Annu. Symp.*, Bethesda, MD, USA: American Medical Informatics Association, 2018, p. 535.
- [28] Y. Zhang, Y. Zhang, S. A. Siddiqui, and A. Kos, "Non-invasive blood-glucose estimation using smartphone ppg signals and subspace knn classifier," *Elektrotehniski Vestnik*, vol. 86, nos. 1–2, pp. 68–74, 2019.
- [29] R. S. Al-Baradie and A. S. C. Bose, "Portable smart non-invasive hemoglobin measurement system," in *Proc. 10th Int. Multi-Conf. Syst., Signals Devices (SSD)*, Mar. 2013, pp. 1–4.
- [30] S. Ramasahayam, S. H. Koppuravuri, L. Arora, and S. R. Chowdhury, "Noninvasive blood glucose sensing using near infra-red spectroscopy and artificial neural networks based on inverse delayed function model of neuron," *J. Med. Syst.*, vol. 39, no. 1, p. 166, Jan. 2015.
- [31] M. D. Anggraeni and A. Fatoni, "Non-invasive self-care anemia detection during pregnancy using a smartphone camera," *IOP Conf. Ser., Mater. Sci. Eng.*, vol. 172, Feb. 2017, Art. no. 012030.
- [32] T. T. Chowdhury, T. Mishma, M. S. Osman, and T. Rahman, "Estimation of blood glucose level of Type-2 diabetes patients using smartphone video," 2019, *arXiv:1911.12619*. [Online]. Available: <http://arxiv.org/abs/1911.12619>
- [33] L. Carroll and T. R. Humphreys, "Laser-tissue interactions," *Clinics Dermatology*, vol. 24, no. 1, pp. 2–7, 2006.
- [34] D. McDuff, S. Gontarek, and R. W. Picard, "Remote detection of photoplethysmographic systolic and diastolic peaks using a digital camera," *IEEE Trans. Biomed. Eng.*, vol. 61, no. 12, pp. 2948–2954, Dec. 2014.
- [35] M. Elgendi, "On the analysis of fingertip photoplethysmogram signals," *Current Cardiol. Rev.*, vol. 8, no. 1, pp. 14–25, Jun. 2012.
- [36] K. Takazawa, N. Tanaka, M. Fujita, O. Matsuoka, T. Saiki, M. Aikawa, S. Tamura, and G. Ibukiyama, "Assessment of vasoactive agents and vascular aging by the second derivative of photoplethysmogram waveform," *Hypertension*, vol. 32, no. 2, pp. 365–370, Aug. 1998.
- [37] U. Rubins, A. Grabovskis, J. Grube, and I. Kukulis, "Photoplethysmography analysis of artery properties in patients with cardiovascular diseases," in *Proc. 14th Nordic-Baltic Conf. Biomed. Eng. Med. Phys.* Berlin, Germany: Springer, 2008, pp. 319–322.
- [38] I. Imanaga, H. Hara, S. Koyanagi, and K. Tanaka, "Correlation between wave components of the second derivative of plethysmogram and arterial Distensibility.," *Jpn. Heart J.*, vol. 39, no. 6, pp. 775–784, 1998.
- [39] S. A. Esper and M. R. Pinsky, "Arterial waveform analysis," *Best Pract. Res. Clin. Anaesthesiology*, vol. 28, no. 4, pp. 363–380, Dec. 2014.
- [40] H. J. Baek, J. S. Kim, Y. S. Kim, H. B. Lee, and K. S. Park, "Second derivative of photoplethysmography for estimating vascular aging," in *Proc. 6th Int. Special Topic Conf. Inf. Technol. Appl. Biomed.*, Nov. 2007, pp. 70–72.
- [41] L. Wang, E. Pickwell-MacPherson, Y. P. Liang, and Y. T. Zhang, "Non-invasive cardiac output estimation using a novel photoplethysmogram index," in *Proc. Annu. Int. Conf. IEEE Eng. Med. Biol. Soc.*, Sep. 2009, pp. 1746–1749.
- [42] E. R. J. Seitsonen, I. K. J. Korhonen, M. J. van Gils, M. Huiku, J. M. P. Lötjönen, K. T. Korttila, and A. M. Yli-Hankala, "EEG spectral entropy, heart rate, photoplethysmography and motor responses to skin incision during sevoflurane anaesthesia," *Acta Anaesthesiologica Scandinavica*, vol. 49, no. 3, pp. 284–292, Mar. 2005.
- [43] Y. Lyu, X. Luo, J. Zhou, C. Yu, C. Miao, T. Wang, Y. Shi, and K.-I. Kameyama, "Measuring photoplethysmogram-based stress-induced vascular response index to assess cognitive load and stress," in *Proc. 33rd Annu. ACM Conf. Hum. Factors Comput. Syst.*, Apr. 2015, pp. 857–866.
- [44] T.-H. Fu, S.-H. Liu, and K.-T. Tang, "Heart rate extraction from photoplethysmogram waveform using wavelet multi-resolution analysis," *J. Med. Biol. Eng.*, vol. 28, no. 4, pp. 229–232, 2008.
- [45] L. Chen, A. T. Reisner, and J. Reifman, "Automated beat onset and peak detection algorithm for field-collected photoplethysmograms," in *Proc. Annu. Int. Conf. IEEE Eng. Med. Biol. Soc.*, Sep. 2009, pp. 5689–5692.
- [46] C. G. Scully, J. Lee, J. Meyer, A. M. Gorbach, D. Granquist-Fraser, Y. Mendelson, and K. H. Chon, "Physiological parameter monitoring from optical recordings with a mobile phone," *IEEE Trans. Biomed. Eng.*, vol. 59, no. 2, pp. 303–306, Feb. 2012.
- [47] E. Jonathan and M. Leahy, "Investigating a smartphone imaging unit for photoplethysmography," *Physiol. Meas.*, vol. 31, no. 11, pp. N79–N83, Nov. 2010.
- [48] H. Yuan, S. F. Memon, T. Neue, E. Lewis, and G. Leen, "Motion artefact minimization from photoplethysmography based non-invasive hemoglobin sensor based on an envelope filtering algorithm," *Measurement*, vol. 115, pp. 288–298, Feb. 2018.
- [49] C. Wei, L. Sheng, G. Lihua, C. Yuquan, and P. Min, "Study on conditioning and feature extraction algorithm of photoplethysmography signal for physiological parameters detection," in *Proc. 4th Int. Congr. Image Signal Process.*, Oct. 2011, pp. 2194–2197.
- [50] A. Chatterjee and A. Prinz, "Image analysis on fingertip video to obtain PPG," *Biomed. Pharmacol. J.*, vol. 11, no. 4, pp. 1811–1827, Dec. 2018.
- [51] A. R. Kavsaoglu, K. Polat, and M. R. Bozkurt, "An innovative peak detection algorithm for photoplethysmography signals: An adaptive segmentation method," *Turkish J. Electr. Eng. Comput. Sci.*, vol. 24, pp. 1782–1796, 2016.
- [52] A. R. Kavsaoglu, K. Polat, and M. R. Bozkurt, "A novel feature ranking algorithm for biometric recognition with PPG signals," *Comput. Biol. Med.*, vol. 49, pp. 1–14, Jun. 2014.
- [53] R. Tiwari and M. P. Singh, "Correlation-based attribute selection using genetic algorithm," *Int. J. Comput. Appl.*, vol. 4, no. 8, pp. 28–34, Aug. 2010.
- [54] J. Koza, "Genetic programming as a means for programming computers by natural selection," *Statist. Comput.*, vol. 4, no. 2, pp. 87–112, Jun. 1994.
- [55] C. C. Aggarwal, "Training deep neural networks," in *Neural Networks and Deep Learning*. Cham, Switzerland: Springer, 2018, pp. 105–167.
- [56] I. Goodfellow, Y. Bengio, and A. Courville. (2016). *Deep Learning. Book in Preparation for Mit Press*. [Online]. Available: <http://www.deeplearningbook.org>
- [57] N. Srivastava, G. Hinton, A. Krizhevsky, I. Sutskever, and R. Salakhutdinov, "Dropout: A simple way to prevent neural networks from overfitting," *J. Mach. Learn. Res.*, vol. 15, no. 1, pp. 1929–1958, 2014.
- [58] V. Dantu, J. Vempati, and S. Srivilliputhur, "Non-invasive blood glucose monitor based on spectroscopy using a smartphone," in *Proc. 36th Annu. Int. Conf. IEEE Eng. Med. Biol. Soc.*, Aug. 2014, pp. 3695–3698.
- [59] S. S. Durduran, "A decision making system to automatic recognize of traffic accidents on the basis of a GIS platform," *Expert Syst. Appl.*, vol. 37, no. 12, pp. 7729–7736, Dec. 2010.
- [60] J. M. Bland and D. G. Altman, "Statistical methods for assessing agreement between two methods of clinical measurement," *Int. J. Nursing Stud.*, vol. 47, no. 8, pp. 931–936, Aug. 2010.



**MD. REZWANUL HAQUE** was born in July 1996. He received the B.Sc. engineering degree in computer science and engineering from the Khulna University of Engineering and Technology, Khulna, Bangladesh. His research interests include bioinformatics, biomedical engineering, health informatics, biomedical instrumentation, computer vision, image processing, natural language processing, machine learning, deep learning, GANs, deep reinforcement learning, and artificial intelligence.



**S. M. TASLIM UDDIN RAJU** was born in Feni, Bangladesh, in 1996. He received the B.Sc. engineering degree in computer science and engineering (CSE) from the Khulna University of Engineering and Technology (KUET), in 2019, where he is currently pursuing the M.Sc. engineering degree.

He is also working as a Lecturer with the CSE Department, KUET. His research interests are in bioinformatics, health informatics, biomedical engineering, deep learning, machine learning, natural language processing, and image processing. He has published some conference papers and journals in these domains. He is also working on some articles about these topics with his students and colleagues.



**MD. ASAF-UDDOWLA GOLAP** received the bachelor's and master's degrees in computer science and engineering from the Khulna University of Engineering and Technology (KUET), Khulna, Bangladesh, in 2017 and 2019, respectively. He is also working as a Lecturer with the Institute of Information and Communication Technology (IICT), KUET. His research interests include bioinformatics, biomedical signal processing, deep learning, machine learning, image processing, genetic programming, and bio-inspired computing techniques.



**M. M. A. HASHEM** received the bachelor's degree in electrical and electronic engineering from the Khulna University of Engineering and Technology (KUET), Khulna, Bangladesh, in 1988, the master's degree in computer science from the Asian Institute of Technology (AIT), Bangkok, Thailand, in 1993, and the Ph.D. degree in artificial intelligence systems from Saga University, Japan, in 1999.

He is currently a Professor with the Department of Computer Science and Engineering, KUET. His research interests include artificial intelligence, machine learning, bioinformatics, biomedical engineering, health informatics, biomedical instrumentation, evolutionary computations, soft computing, and so on. He has published more than 100 refereed articles in international journals/conferences. He is a coauthor of the book *Evolutionary Computations: New Algorithms and their Applications to Evolutionary Robots, Series: Studies in Fuzziness and Soft Computing*, Vol. 147, Springer-Verlag, Berlin/New York, ISBN: 3-540-20901-8, (2004).

...